Ricin A-Chain Activity on Stem−Loop and Unstructured DNA Substrates†

Tim K. Amukele, Setu Roday, and Vern L. Schramm*

Department of Biochemistry, Albert Einstein College of Medicine, 1300 Morris Park Avenue, Bronx, New York 10461

Received December 7, 2004; Revised Manuscript Received January 12, 2005

ABSTRACT: Ricin toxin A-chain (RTA) depurinates a single adenylate on a GAGA stem−loop region of eukaryotic 28S RNA, making it a potent toxin. Steady state rate analysis is used to establish the kinetic parameters for depurination of short RNA, DNA, and RNA−DNA hybrids of GAGA linear segments and stem−loop regions as substrates for RTA. Both stem and tetraloop structures are essential for action on RNA. For DNA stem−loop substrates, stem stability plays a small role in enhancing catalytic turnover but can enhance binding by up to 3 orders of magnitude. DNA sequences of d[GAGA] without stem−loop structures are found to be slow substrates for RTA. In contrast, equivalent RNA sequences exhibit no activity with RTA. Introduction of a deoxyadenosine at the depurination site of short RNA oligonucleotides restores catalytic function. NMR analysis indicates that the short, nonsubstrate GAGA is converted to substrate in GdAGA by the presence of a more flexible ribosyl group at the deoxyadenosine site. Conversion between C2′-endo and C2′-exo conformations at the deoxyadenosine site moves the 3′- and 5′-phosphorus atoms by 1.1 Å, and the former is proposed to place them in a catalytically favorable configuration. The ability to use short RNA−DNA hybrids as substrates for RTA permits exploration of related structures to function as substrates and inhibitors.

Ricin is among the most potent toxins against mammalian cells and has the highest toxicity by injection and inhalation (*1*, *2*). Ricin has been used as a biological weapon [most famously, the "umbrella tip" assassination of the Bulgarian defector Georgi Markov (*3*, *4*)]. Its cytotoxicity has also been harnessed as the toxic component of immunotoxins (*5*, *6*). Clinical trials of ricin toxin A-chain-coupled immunotoxins have resulted in some remarkable remissions; however, the dose-limiting toxicity is a vascular leak syndrome that results in significant morbidity (*7*−*10*). Hence, the potential of RTA[1] antitumor immunotoxin therapy has been considerably constrained (*8*). It may be possible to develop RTA inhibitors as antitoxin rescue agents against ricin toxicity following RTA immunoconjugate therapy. Current attempts at inhibitor design have yielded small molecule RTA inhibitors that bind weakly (millimolar range) (*3*) and more powerful inhibitors (nanomolar range) that are oligonucleotides with 10 or more bases. The previously characterized oligonucleotide stem−loop RNA inhibitors of RTA (*11*, *12*) are unlikely to be orally available and are labile to circulating nucleases (*13*). To explore smaller inhibitor scaffolds, the substrate specificities of small RNA, DNA, and mixed-species oligonucleotides are explored at pH 4.0, the pH optimum for ricin on small stem−loop regions. Other studies have characterized mixed-species loop structures in the context of stem−loop RNA, but at pH 7.5 where reaction rates are too slow to permit a single enzymatic turnover, even at a RTA:RNA molar ratio of 37 (*14*).

RTA inhibits protein translation by depurinating A4324 on a stem−tetraloop GAGA motif of the 28S rRNA, the EF-2 binding site (*15*, *16*). Smaller stem−loop structures retaining the GAGA loop sequence are also substrates (*17*). RTA activity has been characterized on RNA stem−loop regions as a function of stem length and pH (*11*, *18*). These studies showed that RTA experienced a 500-fold increase in its catalytic turnover rate as the number of base pairs in the stem increased from two to five. In addition, the turnover rate of substrates that did not have stable stems could be increased by cross-linking of the termini, indicating that stem formation is important in achieving the RTA transition state with RNA substrates (*11*, *18*). RTA activity on RNA stem−loop regions is also pH-dependent with a maximum at pH 4 and a 100-fold decrease in turnover with every unit change in pH. The extent of productive binding also decreases with increasing pH above pH 4. Short DNA stem−loop regions are also substrates for RTA (*11*). The transition state structures of RNA and DNA stem−loop regions have been characterized, and the results show that RNA and DNA substrates have different geometries at their transition states (*19*, *20*). Results from KIE experiments on A10 and dA10, the RNA and DNA 10mers, respectively, show that the reaction profile for A10 includes an isotope insensitive and rate-limiting step while that for dA10 does not. On chemical reactivity principles, one would expect the turnover rate for dA10 to be higher than that for A10 because dA10 DNA has a 400-fold increased chemical reactivity for depurination relative to RNA. However, this is not the case since RTA catalyzes depurination of dA10 and A10 with a combination

† This work was supported by NIH Research and Training Grants CA72444 and GM07288.

* To whom correspondence should be addressed. Telephone: (718) 430-2777. Fax: (718) 430-8565. E-mail: vern@aecom.yu.edu.

[1] Abbreviations: RTA, ricin toxin A-chain; A12, RNA stem−loop 5′-CGCGGAGACGCG-3′; GNRA, tetraloop sequence family where N is any nucleoside and R is purine; GNNA, tetraloop sequence family where N is any nucleoside; ES, enzyme−substrate complex; d*AX*, DNA stem−loop structure where *X* is total number of nucleosides and the stem length is $(X - 4)/2$ base pairs; T_m, melting temperature.

10.1021/bi0474362 CCC: $30.25
Published on Web 02/25/2005

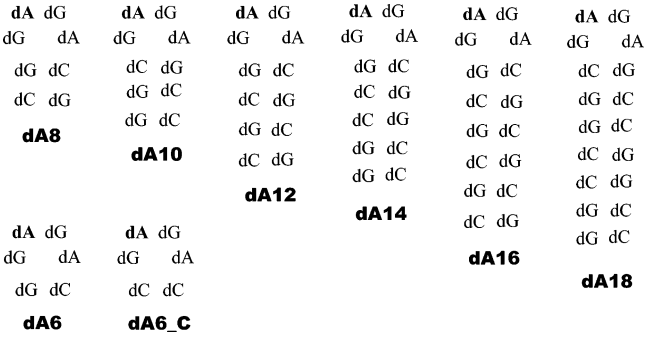

FIGURE 1: Sequences of the deoxyoligonucleotides characterized in this paper.

of leaving group activation and ribooxacarbenium ion generation (*12*). Earlier work using PCR transcription products with radiolabeled adenines reported that RTA slowly hydrolyzes adenine from "random" stretches of single-stranded DNA (*21*, *22*). However, the possibility that these large substrates were capable of forming secondary structures such as GAGA stem−loop regions could not be ruled out. The study of RTA activity on DNA stem−loop structures is necessary to understand this activity (Figure 1).

DNA hairpin structures are involved in recombination (*23*), repair (*24*), transcriptional regulation, and drug interactions (*25*). Studies based on homopolymeric DNA loops showed that thymidine loops with four or five nucleotides are the most stable and all-purine loops such as deoxyadenosine loops are the least stable (*26*). However, certain families of DNA and RNA stem−loop structures are up to 3 kcal/mol more stable than predictions based on size and sequence alone (*27*−*29*). One of these families contains the d[GNNA] tetraloops, the DNA analogues of RNA GNRA loops, a subset of which are substrates for RTA. d[GNNA] stem−loop regions are even more stable than an all-pyrimidine loop (*27*). Stable DNA loops are formed by an extensive hydrogen bonding network (*30*). In addition, the coupling between the loop and the stem is also important in stem−loop stability (*31*). The impact of stem length on the stability of d[GNNA] stem−loop regions has not been studied and would allow comparative assessment of the ability of the d[GNNA] loop to stabilize stem−loop formation.

MATERIALS AND METHODS

General Experimental. RTA was purchased from Sigma. Calf intestinal alkaline phosphatase was purchased from Promega (Madison, WI), and phosphodiesterase I was from Sigma Chemical Co. (St. Louis, MO). DNA oligonucleotides were either synthesized or purchased from Dharmacon Research Inc. All oligonucleotides were HPLC purified using an Xterra C18 reverse phase column using 50 mM ammonium acetate and a linear gradient of methanol. Kinetic results were identical using synthesized or Dharmacon oligonucleotides. Nucleoside phosphoramidites and other reagents for oligoribonucleotide synthesis were purchased from Glen Research (Sterling, VA). Phosphoramidites on CPG solid supports were obtained from ChemGene Corp. (Ashland, MA).

Oligonucleotide Purification and Characterization. Stem−loop DNA oligonucleotides were synthesized on an Expedite 8900 Nucleic Acid Synthesis System from PerSeptive Biosytems, in the trityl-off mode at a 1 μmol scale. Cleavage and deprotection were carried out by incubation in a 3:1 (v/v) NH_4OH/EtOH solution at 55 °C for 3 h. Oligonucleotides were purchased (2′-ACE-protected) from Dharmacon Research. RNA−DNA hybrid oligonucleotides were deprotected essentially as described (Dharmacon manual) except that a 30 min heating protocol was used instead of the recommended 60 min protocol. The oligonucleotides were purified using an Xterra C18 reverse phase column using 50 mM triethylammonium carbonate (pH 6.4) and a linear gradient of 3 to 50% methanol. The integrity of the resulting oligonucleotide was determined using MALDI-TOF mass spectroscopy and by enzymatic digestion followed by HPLC quantitation (*11*). Digests were analyzed on a reversed phase C18 analytical column (WAT011802) eluted using isocratic conditions in 50 mM ammonium acetate (pH 5.0) and 5% MeOH. Nucleoside and deoxynucleoside standards were used to determine the relative amounts of each component in the oligonucleotide digest.

NMR. Oligonucleotides used for NMR studies were at a concentration of 1−2 mM in 50 mM potassium acetate (pH 4) in D_2O at 300 K. The buffer stocks were prepared in D_2O, vacuum-dried, and resuspended in D_2O. The process was repeated twice for each sample. All two-dimensional (2D) experiments were performed on a Bruker DRX 300 spectrometer in D_2O samples at 26 °C. 2D $^1H-^1H$ TOCSY, $^1H-^1H$ DQF COSY, and $^1H-^1H$ NOESY experiments were performed. Presaturation of the residual HOD signal was used for water suppression. TOCSY spectra were collected using a 100 ms MLEV-17 spin lock (*32*), and ROESY and NOESY spectra were collected using a mixing time of 300 ms. Typical spectra were collected with 2K and 512 points in the F_2 and F_1 dimensions, respectively, with 32 scans per t_1 point, a recycle delay of 1.3 s, and a proton sweep width of 14 ppm (D_2O samples) or 30 ppm (H_2O samples) with the carrier set to 4.7 ppm. Spectra were processed with a cosine bell window function and zero-filled to yield data sets with 2K and 512K points in F_2 and F_1, respectively. Proton chemical shifts were referenced to 3-(trimethylsilyl)propionate. Pulsed field gradient NMR (PFG-NMR) was used to determine changes in molecular size. The data obtained from a PFG-NMR study are the decays of the signal with gradient strength. Interpretation of the data to yield structurally significant results requires assumptions which are most applicable to molecules >5 kDa in size that can be represented as spheres or ellipsoids (*33*). However, its applicability can be extended to nonideal systems by the use of model compounds under identical test conditions. dA6 structure at low temperatures was studied using PFG-NMR and a model 6mer dA6_C differing only by a change in the terminal residue from a guanosine to a cytosine. Pulsed field gradient experiments were carried out using the pulse sequence (*34*). Sixteen points were collected from 10 to 90% with a maximal field gradient strength of 60 G/cm.

In $^1H-^1H$ DQF-COSY NMR, each pair of directly bonded protons gives a quartet of peaks. The strength of coupling between these protons is a result of the equilibrium position of the protons and is field-independent. The coupling constant can be obtained by measuring the coupling (in hertz) between cross-peak pairs in each quartet. Residues in the N-conformation (3′-endo) have J(H1H2) constants of <1 Hz, and residues in the S-conformation (2′-endo) have J(H1H2) constants in the 8−10 Hz range (*35*).

Estimation of Errors and Significance of Data. RNA, DNA, and RNA−DNA hybrid oligonucleotides characterized in this study were incubated at 37 °C for more than 10 min before the addition of RTA. The relative kinetic constants in experiments that were carried out simultaneously had typical variations of ±20%. The kinetic parameters reported here are results from individual substrate saturation experiments. The results shown in the tables are the best experiments for representing the trends seen in multiple experiments. The errors shown are the errors of the best fit of the data from the representative experiments. Earlier characterization of RTA showed that RTA has <5% forward commitment for both RNA and DNA stem−loop regions with catalytic turnover numbers encompassing all rates reported here (*19*, *20*). Catalysis is slow relative to substrate equilibration; therefore, the Michaelis constant is known to approximate the dissociation constant for substrates.

Kinetic Analysis for RTA. Assays were carried out essentially as described previously (*11*) except that the reactions were quenched by addition of potassium phosphate (pH 8.0) to give a final concentration of 100 mM. The protein is inactive under these salt and pH conditions. Oligonucleotide concentrations ranged from 10 nM to 0.5 mM, and the amount of RTA used was <15% of the smallest amount of substrate. The maximal amount of conversion to product was <10% of the total initial substrate concentration. RTA was shown to catalyze multiple turnovers on all the substrates characterized in this study. Under these conditions, initial reaction rates were observed when using multiple-time point analysis. The enthalpic and entropic components of the reaction were derived from the slopes of $-\ln k_{cat}$ or $-\ln K_m$ versus $1/T$. The slope of this graph is E_a/R, where E_a is the activation energy and R is the gas constant. E_a is related to H by the equation $E_a = \Delta H^{\ddagger} + RT$, and enthalpy and entropy are related by the equation $\Delta G^{\ddagger} = \Delta H^{\ddagger} - T\Delta S^{\ddagger}$.

Oligonucleotide Thermal Denaturation. Solutions containing each oligonucleotide at 1−30 μM in 10 mM potassium citrate (pH 4.0) and 1 mM EDTA were heated while recording UV spectra. The samples were heated at a rate of 0.5 °C/min and held at each temperature for 2 min before the absorbance was recorded from 3 to 90 °C. Plots of absorbance versus temperature were generated, and the melting temperature was obtained by taking the derivative of the curve and assuming a two-state model. For dA8, dA6, and d(GAGA), the curves were also obtained in a reverse direction, starting at 90 °C and cooling at a rate of 0.5 °C/min with a 30 s incubation at each temperature before the absorbance was recorded. Changes in the absorbance of d(GAGA) as a function of temperature were studied as a control for a completely unstructured oligonucleotide.

RESULTS

Oligonucleotide Thermal Denaturation. All stem−loop oligonucleotides characterized in this study except dA6_C (Table 1) exhibited two-state behavior in their melting transitions, and their T_m's did not vary with concentration in the range of 1−30 μM. This is consistent with their existence primarily as unimolecular hairpins in solution. The T_m's of these stem−loop structures were all ≥15 °C higher than would be predicted using algorithms without consideration of the extrastable nature of these tetraloops. However, the T_m's obtained for these oligonucleotides were similar to those obtained from other stem−loop structures in their (GNRA) class (*27*). The T_m was independent of oligonucleotide concentration, ruling out the possibility of a multimeric species being responsible for the melting phenomena. The T_m's increased with increasing stem length with a plateau at 68 ± 2 °C at ≥4 bp in the stem. The 18mer is an exception to this trend, and the reasons for its lowered relative T_m are not known. One important result was that the 8mer, dA8 with the potential to form only two base pairs in its stem, forms a stable hairpin in solution. The DNA 7mer d[GCG-CACGC], a member of another stable class of loops, is known to form a unimolecular hairpin with a triloop and has a T_m of 76 °C (*36*), providing a precedent for the observation that a hairpin stabilized by just two base pairs can exist as a stable species at elevated temperatures.

Table 1: Kinetic Characterization of DNA Oligonucleotides as Substrates for RTA[a]

substrate	T_m (°C)	k_{cat} (min^{-1})	K_m (μM)	k_{cat}/K_m (M^{-1} s^{-1})
dA-18	61	0.38 ± 0.03	8.8 ± 2	7.2×10^2
dA-16	69	0.26 ± 0.01	2.3 ± 0.6	1.9×10^2
dA-14	67	0.26 ± 0.01	12.4 ± 1.1	6.8×10^2
dA-12	70	0.5 ± 0.04	8.4 ± 1.2	9.9×10^2
dA-10	62	0.25 ± 0.01	12 ± 1.3	3.5×10^2
dA-8	48	0.31 ± 0.03	12.5 ± 4.9	4.1×10^2
dA-6	−	0.32 ± 0.08	94 ± 30	0.56×10^2

[a] Under our experimental conditions, the lower limit for detection of adenine corresponded to a rate of 5×10^{-5} min^{-1}.

dA6 did not provide a well-defined melting curve. However, it gave a plateau at temperatures above 50 °C. This pattern was obtained by heating or cooling and is consistent with dA6 existing as a mixture of structured and unstructured populations at temperatures below 50 °C.

Kinetic Characterization of DNA Stem−Loop Regions. DNA stem−loop regions of varying stem lengths were studied as substrates for RTA (Table 1). k_{cat} did not change significantly as a function of stem length or stability (T_m). All the k_{cat} values were in the range of 0.35 ± 0.15 min^{-1}, and the K_m values, except those of dA16 and dA6, were approximately 10 μM. The K_m for dA16 was 2.3 μM, significantly lower than the K_m for the other stem−loop structures. Formation of the dA16−RTA ES complex is approximately 1 kcal/mol more favorable than formation of other DNA stem−loop complexes. The structural correlates for this observation are unknown. The K_m for dA6 was 94 μM, significantly greater than the K_m for the other stem−loop structures, indicating that formation of a catalytically competent RTA−dA6 complex is 1.3 kcal/mol less favorable. The melting data showed that dA6 exists as two forms under our reaction conditions (37 °C). Since k_{cat} did not change, RTA favors a stem−loop structure for binding but stem stability plays no role in enhancing catalysis on DNA substrates. Conservation of K_m values for DNA stem−loop substrates indicates that although a stem−loop region is required for efficient RTA binding, increasing stem length does not confer additional stability on the RTA−DNA complex. This does not rule out the possibility of a non-stem−loop RTA catalytic route.

Kinetic Characterization of Short DNA Oligonucleotides. The DNA 6mer dA6 has all the functional groups found in the loops of RTA's stem−loop substrates. It explores the

effect of having a structured stem−loop region as opposed to other unstructured conformations for DNA substrates. It has a k_{cat} of 0.32 min^{-1} and a K_m of 94 μM to give a k_{cat}/K_m of 0.56 × 10^2 M^{-1} s^{-1}. Comparison of this result to that obtained for dA8 or dA18 shows an increase in K_m but not in k_{cat} (Table 1).

The K_m for dA6 is approximately 7 times higher than the K_m for other stem−loop substrates (Table 1). If RTA only accepts stem−loop oligonucleotides as substrates, the relative K_m for dA6 would reflect the fraction of dA6 in the stem−loop conformation. However, the K_m for dA6 could also represent an alternative "non-stem−loop" catalytic route for RTA activity of DNA substrates. These possibilities can be resolved by changes in the K_m for dA6 as a function of temperature. The fraction of dA6 that exists as stem−loop structures in solution would be higher at lower temperatures, and its relative K_m might approach those of stable stem−loop structures (represented by dA8) with decreasing temperature. The K_m for dA6 is approximately 9 times that of dA8 at 37 °C, but with decreasing temperature, the K_m values for dA8 and dA6 approach a similar value at 4 °C (Figure 2a). The K_m for dA8 is independent of temperature as predicted for the more stable stem−loop structure.

The enthalpic components of the k_{cat} of dA6 and dA8 were identical at all temperatures (Figure 2b and Table 3), but the enthalpic components of their K_m's (Figure 2c and Table 3) were different, indicating that the k_{cat} steps are thermodynamically identical but that thermodynamics of binding are dependent on the structure (stem−loop or unstructured) of the oligonucleotides. The enthalpic components of catalysis for dA6 and dA8 are 25 and 23 kcal/mol, respectively, similar to those obtained for the solution depurination of adenosine at pH 1, where diprotonated adenine is the leaving group (*37*). This result is consistent with earlier work indicating that RTA catalysis of stem−loop oligonucleotide depurination proceeds via a similar mechanism to acid solvolysis, i.e., an S_N1 mechanism with formation of an oxacarbenium ion transition state followed by addition of water in a separate step (*19*, *20*). The enthalpy for RTA catalysis on the ribosome is estimated to be 10 kcal/mol (*16*). On the basis of these figures, the ribosomal binding proteins contribute 13−15 kcal/mol to catalytic enhancement. However, differences in reaction rates between DNA stem−loop and ribosomal depurination account for approximately 5 kcal/mol. The plots of −ln K_m versus 1/T have two slopes with an inflection point around 10 °C (Figure 2c and Table 4), suggesting a change in the conformation of RTA at low temperatures. This break is also seen with dA6 and dA8, indicating that it resides in RTA dynamics and is not the result of RNA hairpin formation.

These energetics should not be confused with the catalytic efficiency (k_{cat}/k_{chem}) of RTA, which has achieved rates of approximately 1700 min^{-1} on both ribosomes at pH 7.5 and on small stem−loop RNA molecules at pH 4.0 (*17*, *38*).

Diffusion Measurements. Diffusion properties of dA6 and dA6_C were studied at 9 °C using pulsed field gradient NMR (Figure 3). Changes in the signal strength of peaks in the base region (7.4−8.6 ppm) were monitored as a function of field gradient strength. The results were fit to the equation $A_{2\tau}/A_o = \exp(k)$, where A_o and $A_{2\tau}$ are the original and echo signal amplitudes, respectively, and k is the exponential decay constant. The exponential decay constant for each curve is

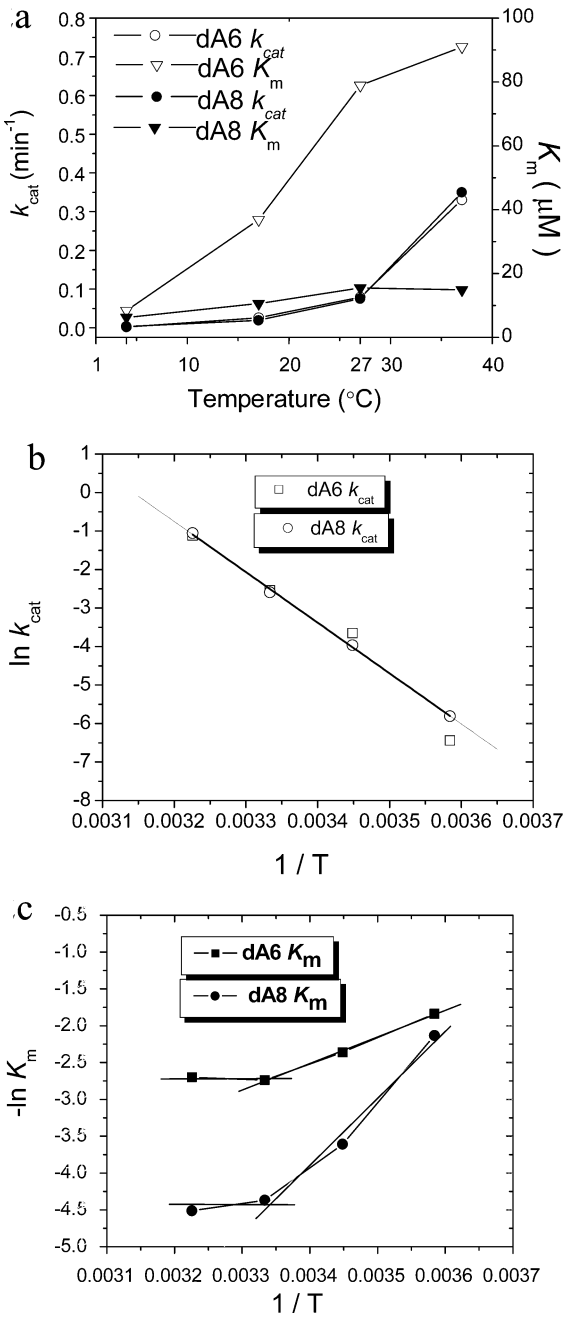

FIGURE 2: k_{cat} and K_m vs temperature, van't Hoff, and Arrhenius plots for RTA activity of dA6 (d[CGAGAG]) and dA8 (d[CGGAGACG]). (a) Kinetic constants for depurination as a function of temperature. The k_{cat} and K_m values were determined by direct fits of the data to Michealis parameters. (b) van't Hoff plots for dA6 and dA8. Fits were derived by least-squares regression analysis of the data. (c) Arrhenius plots for dA6 and dA8. Fits were derived by least-squares regression analysis of the data. The linear portions were drawn by eye to provide the constants in Table 3.

inversely proportional to the diffusion coefficient. When molecular size and solution viscosity are identical, the diffusion coefficient is a direct correlate of the molecular volume. Diffusion plots for dA6 and dA6_C yield a decay constant (k) for dA6 that is 35% less than that for dA6_C. For a hard sphere, a 29% change in the diffusion coefficient corresponds to a 50% reduction in the molecular size (*34*). As the shape of dA6_C is not known, exact changes in molecular volume cannot be established. However, dA6 is significantly more compact under the conditions (pH 4 and 9 °C) than dA6_C, a behavior consistent with G-C base pair

Table 2: Kinetic Parameters for Single-Stranded (non-stem−loop) DNA Oligonucleotides as Substrates for RTA[a]

substrate	k_{cat} (min^{-1})	K_m (μM)	k_{cat}/K_m (M^{-1} s^{-1})
d[GAGA][b]	0.27 ± 0.04	112 ± 36	40
GAGA[b]	$<5 \times 10^{-5}$	>12000[b]	$<7 \times 10^{-3}$
GdAGA	0.18 ± 0.03	65 ± 31	62
d[GAG][b]	>0.02	>300	1.3
d[GA][b]	$<5 \times 10^{-5}$	−	−

[a] Under our experimental conditions, the lower limit for detection of adenine corresponded to a rate of 5×10^{-5} min^{-1}. [b] These names represent the full sequences of these oligonucleotides.

Table 3: van't Hoff Analysis of RTA Reaction on dA6 and dA8

	temp (°C)	ΔG_{ES}	ΔH_{ES}	$T\Delta S_{ES}$ (kcal/mol)	ΔG	ΔH	$T\Delta S$ (kcal/mol)
dA6	4	−6.28	0.08[a]	6.36[b]	0.7	25.5	24.8
	17	−7.18	0.08[a]	7.26[b]	1.6	25.4	23.8
	27	−5.7	−6.53	−0.8	2.24	25.3	23.1
	37	−5.8	−6.53	−0.72	3.96	25	21
dA8	4	−7.04	−2.83[a]	4.2[b]	0.65	25.5	25
	17	−7.37	−2.83[a]	4.5[b]	1.6	25.4	24
	27	−6.8	−17.2	−10.4	2.4	25.3	23
	37	−6.8	−17.2	−10.4	3.6	25	21.4

[a] Upper limits of these values. [b] Lower limits of these values.

Table 4: Coupling Constants (Hz) between the H1′ and H2′ Protons in d[GAGA], GdAGA, and GAGA[a]

	d[GAGA]	GdAGA	GAGA
spin system 1	8.7	8.3	4.5
spin system 2	9.0	4.1	4.5
spin system 3	9.4	5.6	4.5
spin system 4	8.7	6.4	4.5

[a] The values in the table were obtained from 1D ^1H spectra recorded at 300 MHz and from the H1′−H2′ cross-peaks in 2D DQF-COSY spectra. The data were compared with known nucleoside NMR conformational analysis data (*35*). The base in spin systems 1 and 3 is adenine and in spins systems 2 and 4 guanine.

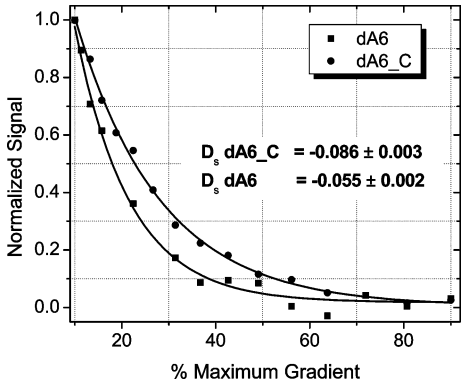

FIGURE 3: Comparison of NMR "intensity decay" curves for dA6 (d[CGAGAG]) and dA6_C (d[CGAGAC]) in 50 mM potassium acetate (pH 4) in D_2O at 9 °C.

and formation of a stem−loop region. For dA6, two of the nine peaks studied in the diffusion study have decay characteristics similar to those of dA6_C, while the other peaks have decay characteristics that are the result of a more compact species. Thus, dA6 exists as a mixture of stem−loop and unstructured DNA even at low temperatures. The dA6 peaks used for the diffusion study have not been assigned due to crowding and line broadening at low temperatures.

Kinetic Characterization of RTA Activity on Unstructured Oligonucleotides. At higher temperatures, dA6 is unstructured; however, it was not clear if the elevated K_m at higher temperatures represented the fraction of dA6 in a stem−loop conformation or if it reflected the K_m of an alternative non-stem−loop RTA catalytic route. To distinguish between these possibilities, d[GAGA] was synthesized and tested as a substrate for RTA. The 4mer d[GAGA] is a substrate for RTA with a k_{cat} of 0.27 min^{-1}, a K_m of 112 μM, and a k_{cat}/K_m of 40 M^{-1} s^{-1} (Table 2). Although the k_{cat}/K_m for RTA is 15 500 times better on its most efficient substrate, A12 (*11*), the turnover rate for d[GAGA] at pH 4 is 10^5 times faster than the intrinsic rate of acid-catalyzed depurination of deoxyadenosine at pH 1 (*37*).

Kinetic constants for RTA action on d[GAGA] are similar to that of dA6 with k_{cat}/K_m ratios of 62 and 56 M^{-1} s^{-1}, respectively. The RNA GAGA 4mer is not a substrate for RTA within the limits of detection of our system (5×10^{-6} min^{-1}). The ratio of the turnover rate of d[GAGA] to that of GAGA is >5400 [k_{cat}(d[GAGA])/k_{cat}(GAGA)] and represents a difference of >5.3 kcal/mol in the additional energetic barrier for GAGA catalysis. GAGA was used as a competitive inhibitor of both dA8 (d[CGGAGACG]) and d[GAGA] to determine if it binds RTA. There was no inhibition of either substrate at GAGA concentrations of up to 3 mM. Hence, at least 2 kcal/mol {RT ln[K_m(d[GAGA])/K_i(GAGA)]} of the reduced GAGA catalysis relates to inefficiency in forming the Michaelis complex. The substrate groups responsible for the difference in catalytic activity between GAGA and d[GAGA] were explored with GdAGA. Deletion of this hydroxyl alone conferred a >3600-fold (5 kcal/mol) increase in substrate activity, to give a substrate with k_{cat}, K_m, and k_{cat}/K_m values of 0.18 min^{-1}, 65 μM, and 62 M^{-1} s^{-1} (Table 2). These kinetic characteristics are similar to those of d[GAGA]. Similar binding and transition state energetics in short tetrameric RNA−DNA sequences require a deoxynucleoside only at the depurination site.

The k_{cat} for d[GAGA] is similar to that of larger DNA stem−loop substrates. The minimal DNA substrate for RTA activity was explored with d[GAG], d[AGA], and d[GA]. The 3mer d[GAG] is a substrate for RTA and gave a linear increase in the turnover rate with increasing substrate concentration up to 300 μM. The k_{cat}/K_m value was determined from the initial slope to be 1.8 M^{-1} s^{-1}. Lower limits for k_{cat} and K_m of d[GAG] were 0.016 min^{-1} and 150 μM, respectively. The catalytic efficiency of d[GAG] is 5% of that of d[GAGA] as indicated by their relative k_{cat}/K_m values. Binding affinity contributes to this reduction in catalytic productivity, making K_m a significant contributor to the reduced k_{cat}/K_m. Its lower limit is greater than twice the K_m value for d[GAGA]. The increased K_m may be due to the loss of specific group interactions that are important in binding or could be due to an unfavorable substrate conformation since significant base stacking can occur even in dinucleosides (*39*).

The slow turnover rate for d[GAG] required controls to show that RTA was causing adenine depurination. RTA catalyzed multiple catalytic turnovers on d[GAG] and retained full activity when incubated with stem−loop RNA substrates at the end of the incubation. The reaction products were analyzed by digestion and reverse phase HPLC and exhibited the expected profiles. The slow turnover rate and

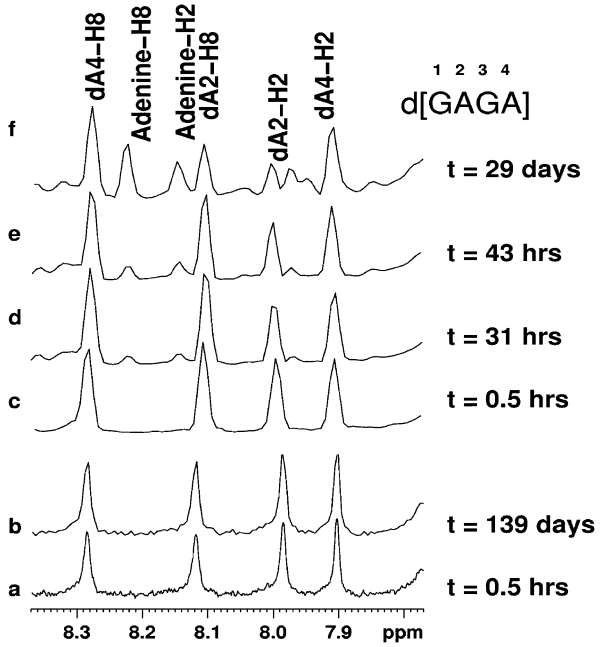

FIGURE 4: NMR spectral signature of d[GAGA] and substrate activity with RTA. Samples were analyzed at room temperature with a Bruker 600 NMR spectrometer. Traces a and b are spectra of 1 mM d[GAGA] alone in 50 mM potassium acetate (pH 4). Traces c−f are spectra of 0.8 mM d[GAGA] with 24 μM RTA in 50 mM potassium acetate (pH 4) and 35 mM potassium chloride, incubated for the times shown.

high K_m for d[GAG] did not allow full conversion of the substrate to the product. The DNA 3mer d[AGA] was not a substrate for RTA within the limits of detection (5×10^{-6} min^{-1}) at 500 μM.

RTA Specificity on Unstructured Oligonucleotides. RTA has been reported to cleave the first adenine site of the tetraloop of dA-10 100 times more efficiently than the second site, as measured by their relative k_{cat}/K_m ratios (*19*). The specificity for RNA stem−loop structures (A10) is absolute for the first adenine of the tetraloop. To determine if RTA retained its specificity with d[GAGA], the depurination reaction was followed by NMR analysis (Figure 4). Spectra a and b are control samples of d[GAGA] at 30 min and 139 days in the absence of RTA. The nonenzymatic depurination rate is negligible. Spectra c−f demonstrate release of adenine specifically from the first adenine of d[GAGA] as indicated by decreases in both the dA2 H2 and dA2 H8 peak intensities and new peaks corresponding to H2 and H8 of free adenine. The slow rates (at 29 days) resulted from conditions (8-fold higher salt concentration and reaction at 4 °C) that facilitated RTA stability. These turnover rates still represent a 10000-fold rate enhancement over the uncatalyzed rate of deoxyadenosine depurination at pH 1. The NMR experiment demonstrates that RTA retains its specificity with d[GAGA].

Structural Differences between GAGA and GdAGA. The DQF-COSY spectrum of GdAGA gives a quartet of cross-peaks for protons on adjacent carbons (Figure 5). Coupling between peaks is the result of the equilibrium positions of the respective protons. The two most diagnostic torsion angles for determining furanose ring conformations in nucleosides are the H1′−C−C−H2′ and H3′−C−C−H4′ angles. 3′-Endo and 2′-endo conformations in nucleosides are known to result in H1′−H2′ coupling constants of <1 and 8−10 Hz, respectively (*35*). One-dimensional (1D) and

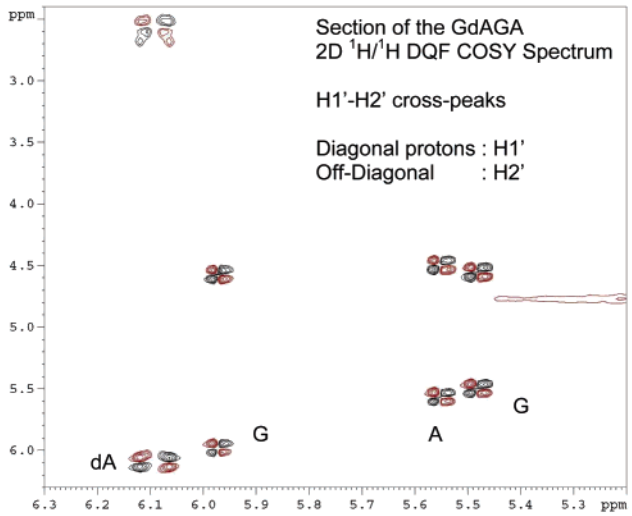

FIGURE 5: 2D ^{1}H−^{1}H DQF COSY spectrum of GdAGA in 50 mM potassium acetate (pH 4) on a Bruker 300 MHz spectrometer at 26 °C in D_2O. H1′−H2′ cross-peaks are centered at 6.09, 5.98, 5.56, and 5.48 ppm for spin systems 1−4, respectively. The base in spin systems 1 and 3 is adenine, and that in systems 2 and 4 is guanine. The larger H1′−H2′ coupling constant for 2′-deoxyadenosine is clearly distinguishable from that of the ribose residues in this sequence.

2D DQF-COSY spectra were collected for GAGA, GdAGA, and d[GAGA] to establish ribosyl conformations. All the nucleoside ribosyl groups in GAGA and the three RNA ribosyl groups of GdAGA had $^3J_{H1'-H2'}$ coupling constant values that ranged between 4.5 and 5.5 Hz (Table 4). These values suggest that the ribose rings are in dynamic equilibrium between the 2′- and 3′-endo forms. However, the 2′-deoxyadenosine in GdAGA had a H1′−H2′ coupling constant of 8.7 Hz which clearly establishes a preference for the 2′-endo conformation. This is the adenosine hydrolyzed in the RTA-catalyzed reaction and suggests a preference of RTA for the reactive residue to be in a 2′-endo conformation. However, differences in flexibility between GAGA and GdAGA and a role for flexibility in catalysis cannot be ruled out.

Effect of pH on RTA Activity with DNA Oligonucleotides. RTA activity on dA14 and d[GAGA] was characterized as a function of pH. Both binding and catalysis of DNA oligonucleotides are affected by pH (Figure 6). The K_m decreases with a lower pH to a plateau of 77 nM below pH 3.0. The K_m value is dependent on the protonation of one group with a pK of 5.0 ± 0.1, and the k_{cat} is dependent on the protonation of one group with a pK of 3.2 ± 0.5. The identity of the groups through which these effects (k_{cat} and K_m) are mediated is not known and could be enzyme or substrate groups. The slope of the line defining the relationship between k_{cat} and K_m is 1, indicating that the effect we observe is due to protonation of a single group.

DISCUSSION

RTA Does Not Require Stem−Loop Structure for Catalytic Activity on DNA. RTA acts on both stem−loop and non-stem−loop DNA substrates to give similar k_{cat} but dissimilar K_m values. Stem−loop structures bind up to 3 orders of magnitude more tightly. d[GAGA] has a k_{cat} similar to that of DNA stem−loop substrates. For RTA activity on DNA substrates, functional groups outside the tetraloop, including

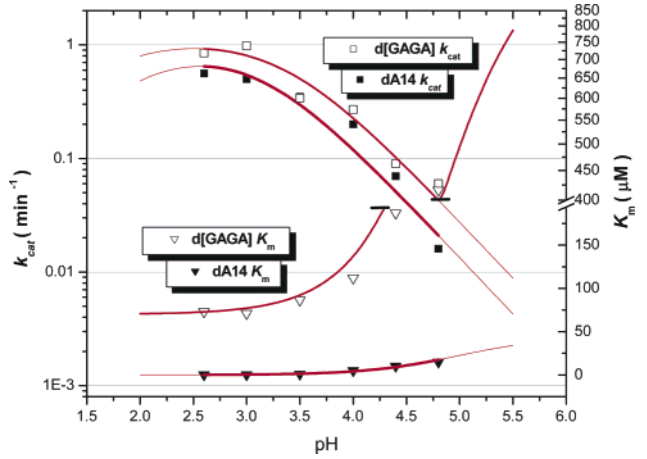

FIGURE 6: Effect of pH on k_{cat} and K_m for RTA activity on dA14 and d[GAGA]. The lines represent the best fits of the data to the equations $k_{cat}^{app} = k_{cat}(1 + [H^+]/K_a)$ and $K_m^{app} = K_m(1 + K_a/[H^+])$, respectively.

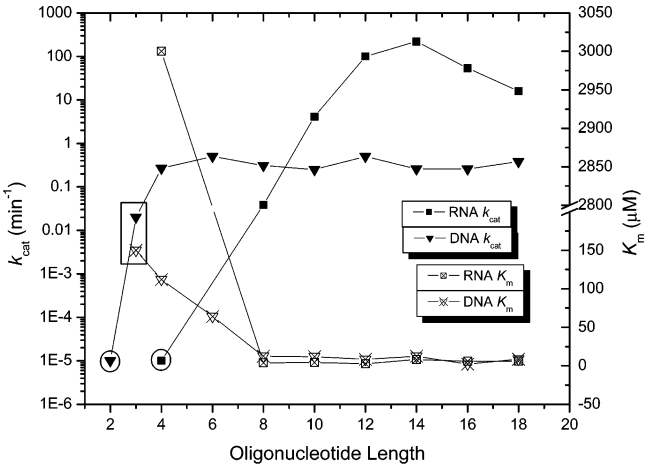

FIGURE 7: Kinetic parameters for RTA acting on DNA and RNA oligonucleotides of different lengths. No significant activity was seen for the values enclosed in circles, and the values represent the limit of detection of the assay. For the DNA 3mer d[GAG] (enclosed in a rectangle), the values represent the lower and upper limit, respectively, for k_{cat} and K_m of d[GAG]. An RNA oligonucleotide of 10 bases has the sequence 5′-GCGGAGACGC-3′ with the central GAGA portion forming the tetraloop.

the flanking phosphates, do not play a role in transition state stabilization but only in optimizing binding. The catalytic model is that the stem provides a scaffold for folding of the tetraloop which then can bind efficiently.

This is not the case for RNA stem−loop substrates. Kinetic constants comparing RNA and DNA stem−loop substrates demonstrate the following. (1) For RNA substrates, there is a 500-fold increase in the turnover rate as the number of base pairs in the stem goes from two to five (*11*, *18*) (Figure 7). (2) For DNA substrates in the 2−5 bp range, the k_{cat} and K_m values are similar. The k_{cat} for DNA substrates drops significantly when the oligonucleotide substrates lose the tetraloop. The K_m for stem−loop DNA substrates is constant until the oligonucleotide loses the ability to form a stem−loop structure at 37 °C. RTA is most active on RNA substrates with ≥3 bp in the stem (Figure 7). Below this range, it is more catalytically active on DNA substrates. In a comparison of k_{cat} values for RNA and DNA substrates, RTA shows a preference for RNA for stem−loop nucleotides. In contrast, k_{cat} is greater for DNA than RNA for the GAGA sequence without the stabilizing stem−loop structure. The mechanism of this preference awaits additional structural studies. However, the TS-stabilizing ability of the stem is mediated through some RNA-specific quality. It is also not known if this property resides in a single residue or if it depends on the entire stem and loop being ribosugars. Additional studies of the activity of RNA−DNA hybrid stem−loop structures as a function of stem length will be needed to resolve this issue.

The relationship between pH and activity is also different for DNA and RNA stem−loop structures (A10 and A14). For RNA stem−loop structures; the relationships between pH and the log of both k_{cat} and K_m have slopes of 2. Thus, both k_{cat} and K_m are affected by the protonation of two groups which each accept a proton. This is not the case for dA14 and d[GAGA]. Both k_{cat} and K_m for dA14 and d[GAGA] involve protonation of a single group. This suggests that the second group is a protein group specific for RNA catalysis. The pK values for all group(s) that affect RTA activity on DNA and RNA stem−loop structures converge near pH 4. The structure of RTA bound to adenine and mono- and dinucleosides, sequence alignment, and mutational studies have implicated two acidic residues, Glu177 and Asp96, in RTA's catalytic mechanism. Both have solution pK_a values near 4. In addition, the pK_a's of N1 and N3 of adenine are around pH 4. However, the pK_a values of these groups can be significantly altered by the catalytic site environment, and group assignments have not yet been made.

Role of the Stem in RTA Catalysis. For RNA stem−loop structures, the stability of the stem enhances both binding and catalysis, while for DNA stem−loop structures, stem stability plays no role in enhancing binding or catalysis. Comparison of A12 and A12_6dA as RTA substrates showed that deoxyadenosine at the depurination site resulted in a 1.6 kcal/mol less favorable binding (K_m) and 1.83 kcal/mol greater k_{cat}. In the case of GAGA and GdAGA, deoxyadenosine increased the extent of binding (K_m) and k_{cat} by >2.3 and >2.7 kcal/mol, respectively. Since GAGA does not bind RTA, GdAGA must have structural properties more suited to binding. NMR analysis indicates that GAGA and GdAGA differ with respect to the ribose ring conformation at the reactive residue. The 3′-phosphorus−5′-phosphorus distances differ considerably at residues with 3′-endo or 2′-endo nucleosides. This difference of 1.1 Å (7.0 Å vs 5.9 Å) is sufficient to disrupt the H-bond interactions with RTA (Figure 8) (*38*). Crystal structures of small RNA stem−loop structures from the ricin depurination sites of rat 28s rRNA (*40*) and *Escherichia coli* 23s rRNA (*41*) sarcin loops demonstrate a >1 Å increase in inter-phosphate distance for the phosphates flanking the two middle residues as compared to those flanking the first and last residues of both tetraloops. NMR structures of GAGA stem−loop regions do not demonstrate this phenomenon (*43*) because NMR data do not adequately define the position of the backbone phosphates. This helps to explain the different roles of the stem in RTA catalysis of RNA versus DNA stem−loop structures. For RNA stem−loop regions, the stability of the stem enhances both binding and catalysis, while for DNA stem−loop regions, stem stability does not play a significant role in enhancing binding or catalysis. These results suggest that RNA stems stabilize the inter-phosphate distances that RTA requires for tetraloop binding. This requirement does not exist

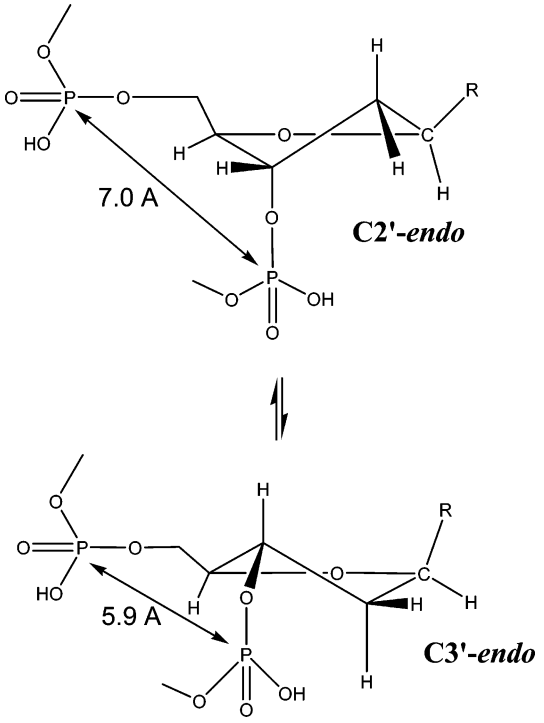

FIGURE 8: Comparison of 2′-endo (trans phosphate) and 3′-endo (gauche phosphates) 2′-deoxyribonucleosides, showing differences in inter-phosphate distances. The distances were obtained from crystal structures of the relevant nucleosides (*38*).

for DNA because it can achieve the optimal inter-phosphate distance without assistance from a stem. This may explain why RTA prefers RNA over DNA stems independent of the loop constituents. RNA stems are wider and less flexible than DNA stems, two characteristics that would be advantageous in loop "stretching". This requirement for an optimal inter-phosphate distance is a well-known feature of other enzymes that interact with diphosphorylated ribosyl groups (*43*), including adenine phosphoribosyltransferase (*44*).

Inhibitor Design. dA14 is shown to bind most tightly at pH <4, where N1 or N3 of the A-depurination site might be protonated. Incorporation of a purine analogue with an elevated pK_a at these positions might be anticipated to increase binding affinity. The goal of inhibitor and substrate design for RTA is ultimately for use in a biological context at neutral pH. Hence, effective inhibitors will need to retain binding activity at neutral pH. DNA stem−loop substrates exhibit a dependence of a single group (pK_a = 4.0), while RNA substrates depend on two groups and therefore suffer loss of binding 10-fold more rapidly as the pH is increased. It is advantageous to use inhibitors in a DNA context because of this property.

DNA substrates for RTA do not require a stem or other functional groups outside the tetraloop. This holds promise for the use of small DNA oligonucleotides as scaffolds for the design of transition state analogue inhibitors of RTA. Catalysis by RTA with A12_6dA is 3600-fold more efficient than dA12, but both 4mer analogues GdAGA and d[GAGA] have similar binding and turnover kinetic profiles. Since transition state analogue binding affinity is limited by the k_{cat}/k_{chem} ratio, mimics of slow substrates, like unstructured DNAs, have less potential for tight binding. However, it should be remembered that the k_{cat}/k_{chem} for ricin is approximately 10^{12} on either ribosomes or stem−loop RNA under conditions of optimal pH and RNA sequence, providing a large energetic potential for binding of transition state analogues. The use of cross-linking agents to mimic the width and stiffness of an RNA stem may permit the re-acquisition of catalytic potential of the GdAGA loop configuration. The finding that d[GAG] is a minimal substrate for RTA provides additional flexibility for analogue design. Finally, the altered pH optimum for stem−loop structures (pH 4) relative to ribosomes (pH 7.5) suggests that the enzyme alters the pK_a of an RTA catalytic site residue or the substrate, parameters which need additional definition as part of understanding catalytic site binding interactions.

DNA GNRA Loops. Both RNA GNRA and DNA GNNA tetraloops are stable, with melting temperatures 15−25 °C higher than those of similar stem−loop structures with different loop sequences. d[GNNA] tetraloops have been shown to be expanded d[cGNAg] loops (*28*, *31*). Comparison of dA8 and d[ggGCAcc] with T_m's of 48 and 50 °C, respectively, indicates that there is little energetic cost for insertion of a residue between the second and third positions of a d[gGCAc] triloop (*31*).

A d[GNRA] loop can stabilize stem−loop structures by up to 3 kcal/mol. However, the ability to stabilize stem−loop structures as a function of stem length has not been reported. This loop sequence stabilizes formation of stem−loop regions independent of stem length. The lower size limit for hairpin formation is a 5mer for a single-base loop hairpin and a 6mer for a four-base loop. The smallest single-base loop stem−loop structure identified to date is a 7mer with a melting temperature of 76 °C, a transcriptional regulatory element (*45*, *46*). However, there has been no prior evidence of hairpin formation in a 6mer oligonucleotide. The diffusional NMR study of dA6 versus dA6_C demonstrates that at 9 °C dA6 is significantly more compact than dA6_C, a 6mer analogue that is incapable of forming a hairpin structure. In addition, the low K_m of dA6 at 4 °C in comparison to the K_m values obtained using more stable hairpin substrates suggests that dA6 exists primarily as a hairpin at this temperature.

CONCLUSIONS

(1) GNNA stem−loop structures in a DNA context are highly stable with the ability to form stable hairpin structures even in oligonucleotides at the theoretical minimal size limit for formation of stem−loop structures. (2) Both the k_{cat} and K_m for RTA with DNA substrates, irrespective of the presence of a stem, are dependent on the protonation of single groups. In contrast, RTA acting on RNA shows that both k_{cat} and K_m are dependent on two ionizable groups. (3) RTA catalyzes adenine depurination on unstructured (non-stem−loop) DNA oligonucleotides with a k_{cat} similar to that on stem−loop oligonucleotides and with retention of the GAGA specificity. (4) The smallest RTA substrate is the 3mer d[GAG]. (5) The stem in RNA stem−loop structures stabilizes the two middle loop residues into an optimal inter-phosphate distance for RTA binding. DNA substrates can adopt this conformation without stabilization from the stem; hence, RNA substrates for RTA require stable stems, and DNA substrates with and without stems are accepted as substrates. The action of RTA on DNA substrates may facilitate the design of novel RTA inhibitors and substrate molecules.

ACKNOWLEDGMENT

We thank Dr. Sean Cahill at the Albert Einstein College of Medicine Structural NMR Center. The instrumentation in the AECOM Structural NMR Resource is supported by the Albert Einstein College of Medicine and in part by grants from the NSF Academic Research Infrastructure Program (DBI9601607) and Howard Hughes Medical Institute Research Resources for Biomedical Sciences.

REFERENCES

1. Fodstad, O., Olsnes, S., and Pihl, A. (1976) Toxicity, distribution and elimination of the cancerostatic lectins abrin and ricin after parenteral injection into mice, *Br. J. Cancer 34*, 418−425.
2. Wilhelmsen, C. L., and Pitt, M. L. (1996) Lesions of acute inhaled lethal ricin intoxication in rhesus monkeys, *Vet. Pathol. 33*, 296−302.
3. Miller, D. J., Ravikumar, K., Shen, H., Suh, J. K., Kerwin, S. M., and Robertus, J. D. (2002) Structure-based design and characterization of novel platforms for ricin and shiga toxin inhibition, *J. Med. Chem. 45*, 90−98.
4. Crompton, R., and Gall, D. (1980) Georgi Markov: Death in a pellet, *Med.-Leg. J. 48*, 51−62.
5. Ghetie, V., and Vitetta, E. S. (2001) Chemical construction of immunotoxins, *Mol. Biotechnol. 18*, 251−268.
6. Vitetta, E. S. (1990) Immunotoxins: New therapeutic reagents for autoimmunity, cancer, and AIDS, *J. Clin. Immunol. 10*, 15S−18S.
7. Baluna, R., Coleman, E., Jones, C., Ghetie, V., and Vitetta, E. S. (2000) The effect of a monoclonal antibody coupled to ricin A chain-derived peptides on endothelial cells in vitro: Insights into toxin-mediated vascular damage, *Exp. Cell Res. 258*, 417−424.
8. Baluna, R., and Vitetta, E. S. (1997) Vascular leak syndrome: A side effect of immunotherapy, *Immunopharmacology 37*, 117−132.
9. Schnell, R., Vitetta, E., Schindler, J., Barth, S., Winkler, U., Borchmann, P., Hansmann, M. L., Diehl, V., Ghetie, V., and Engert, A. (1998) Clinical trials with an anti-CD25 ricin A-chain experimental and immunotoxin (RFT5-SMPT-dgA) in Hodgkin's lymphoma, *Leuk. Lymphoma 30*, 525−537.
10. Engert, A., Diehl, V., Schnell, R., Radszuhn, A., Hatwig, M. T., Drillich, S., Schon, G., Bohlen, H., Tesch, H., Hansmann, M. L., Barth, S., Schindler, J., Ghetie, V., Uhr, J., and Vitetta, E. (1997) A phase-I study of an anti-CD25 ricin A-chain immunotoxin (RFT5-SMPT-dgA) in patients with refractory Hodgkin's lymphoma, *Blood 89*, 403−410.
11. Chen, X. Y., Link, T. M., and Schramm, V. L. (1998) Ricin A-chain: Kinetics, mechanism, and RNA stem-loop inhibitors, *Biochemistry 37*, 11605−11613.
12. Tanaka, K. S., Chen, X. Y., Ichikawa, Y., Tyler, P. C., Furneaux, R. H., and Schramm, V. L. (2001) Ricin A-chain inhibitors resembling the oxacarbenium ion transition state, *Biochemistry 40*, 6845−6851.
13. Lipinski, C. A., Lombardo, F., Dominy, B. W., and Feeney, P. J. (2001) Experimental and computational approaches to estimate solubility and permeability in drug discovery and development settings, *Adv. Drug Delivery Rev. 46*, 3−26.
14. Orita, M., Mishikawa, F., Kohno, T., Senda, T., Mitsui, Y., Endo, Y., Taira, K., and Nishikawa, S. (1996) High-resolution NMR study of a GdAGA tetranucleotide loop that is an improved substrate for ricin, a cytotoxic plant protein, *Nucleic Acids Res. 24*, 611−618.
15. Endo, Y., Mitsui, K., Motizuki, M., and Tsurge, K. (1987) The mechanism of action of ricin and telated toxic lectins on eukaryotic ribosomes. The site and the characteristics of the modification in 28S ribosomal RNA caused by the toxins, *J. Biol. Chem. 262*, 5908−5912.
16. Montanaro, L., Sperti, S., Mattioli, A., Testoni, G., and Stirpe, F. (1975) Inhibition by ricin of protein synthesis in vitro. Inhibition of the binding of elongation factor 2 and of adenosine diphosphate-ribosylated elongation factor 2 to ribosomes, *Biochem. J. 146*, 127−131.
17. Gluck, A., Endo, Y., and Wool, I. G. (1992) Ribosomal RNA identity elements for ricin A-chain recognition and catalysis. Analysis with tetraloop mutants, *J. Mol. Biol. 226*, 411−424.
18. Allerson, C. R., and Verdine, G. L. (1995) Synthesis and biochemical evaluation of RNA containing an intrahelical disulfide cross-link, *Chem. Biol. 2*, 667−675.
19. Xiang-Yang, C., Berti, P. J., and Schramm, V. L. (2000) Transition-State Analysis for Depurination of DNA by Ricin A-Chain, *J. Am. Chem. Soc. 122*, 6527−6534.
20. Xiang-Yang, C., Berti, P. J., and Schramm, V. L. (2000) Ricin A-Chain: Kinetic Isotope Effects and Transition State Structure with Stem-Loop RNA, *J. Am. Chem. Soc. 122*, 1609−1617.
21. Barbieri, L., Bolognesi, A., Valbonesi, P., Polito, L., Olivieri, F., and Stirpe, F. (2000) Polynucleotide: Adenosine glycosidase activity of immunotoxins containing ribosome-inactivating proteins, *J. Drug Targeting 8*, 281−288.
22. Brigotti, M., Barbieri, L., Valbonesi, P., Stirpe, F., Montanaro, L., and Sperti, S. (1998) A rapid and sensitive method to measure the enzymatic activity of ribosome-inactivating proteins, *Nucleic Acids Res. 26*, 4306−4307.
23. Gellert, M. (2002) V(D)J recombination: RAG proteins, repair factors, and regulation, *Annu. Rev. Biochem. 71*, 101−132.
24. Lenzmeier, B. A., and Freudenreich, C. H. (2003) Trinucleotide repeat instability: A hairpin curve at the crossroads of replication, recombination, and repair, *Cytogenet. Genome Res. 100*, 7−24.
25. Wadkins, R. M. (2000) Targeting DNA secondary structures, *Curr. Med. Chem. 7*, 1−15.
26. Haasnoot, C. A., de Bruin, S. H., Berendsen, R. G., Janssen, H. G., Binnendijk, T. J., Hilbers, C. W., van der Marel, G. A., and van Boom, J. H. (1983) Structure, kinetics and thermodynamics of DNA hairpin fragments in solution, *J. Biomol. Struct. Dyn. 1*, 115−129.
27. Antao, V. P., Lai, S. Y., and Tinoco, I., Jr. (1991) A thermodynamic study of unusually stable RNA and DNA hairpins, *Nucleic Acids Res. 19*, 5901−5905.
28. Nakano, M., Moody, E. M., Liang, J., and Bevilacqua, P. C. (2002) Selection for thermodynamically stable DNA tetraloops using temperature gradient gel electrophoresis reveals four motifs: d(cGNNAg), d(cGNABg), d(cCNNGg), and d(gCNNGc), *Biochemistry 41*, 14281−14292.
29. Antao, V. P., and Tinoco, I., Jr. (1992) Thermodynamic parameters for loop formation in RNA and DNA hairpin tetraloops, *Nucleic Acids Res. 20*, 819−824.
30. Moody, E. M., and Bevilacqua, P. C. (2003) Folding of a stable DNA motif involves a highly cooperative network of interactions, *J. Am. Chem. Soc. 125*, 16285−16293.
31. Moody, E. M., and Bevilacqua, P. C. (2003) Thermodynamic coupling of the loop and stem in unusually stable DNA hairpins closed by CG base pairs, *J. Am. Chem. Soc. 125*, 2032−2033.
32. Bax, A., and Davis, D. G. (1985) MLEV-17-Based Two-Dimensional Homonuclear Magnetization Transfer Spectroscopy, *J. Magn. Reson. 65*, 355.
33. Teller, D. C., Swanson, E., and de Haen, C. (1979) The translational friction coefficient of proteins, *Methods Enzymol. 61*, 103−124.
34. Wu, D., Chen, A., and Johnson, C. S. (1995) An Improved Diffusion-Ordered Spectroscopy Experiment Incorporating Bipolar-Gradient Pulses, *J. Magn. Reson., Ser. A 115*, 260−264.
35. Marino, J. P., Schwalbe, H., and Griesinger, C. (1999) *J*-Coupling Restraints in RNA Stucture Determination, *Acc. Chem. Res. 32*, 614−623.
36. Hirao, I., Kawai, G., Yoshizawa, S., Nishimura, Y., Ishido, Y., Watanabe, K., and Miura, K. (1994) Most compact hairpin-turn structure exerted by a short DNA fragment, d(GCGAAGC) in solution: An extraordinarily stable structure resistant to nucleases and heat, *Nucleic Acids Res. 22*, 576−582.
37. Garrett, E. R., and Mehta, P. J. (1972) Solvolysis of adenine nucleosides. I. Effects of sugars and adenine substituents on acid solvolyses, *J. Am. Chem. Soc. 94*, 8532−8541.
38. Amukele, T. K., and Schramm, V. L. (2004) Ricin A-chain substrate specificity in RNA, DNA and hybrid stem-loop structures. *Biochemistry 43*, 4913−4922.
39. Lee, C. H., Charney, E., and Tinoco, I., Jr. (1979) Conformations of dinucleoside phosphates in aqueous solution, *Biochemistry 18*, 5636−5641.
40. Correll, C. C., Munishkin, A., Chan, Y. L., Ren, Z., Wool, I. G., and Steitz, T. A. (1998) Crystal structure of the ribosomal RNA domain essential for binding elongation factors, *Proc. Natl. Acad. Sci. U.S.A. 95*, 13436−13441.

41. Correll, C. C., Wool, I. G., and Munishkin, A. (1999) The two faces of the *Escherichia coli* 23 S rRNA sarcin/ricin domain: The structure at 1.11 Å resolution, *J. Mol. Biol. 292*, 275−287.
42. Jucker, F. M., Heus, H. A., Yip, P. F., Moors, E. H., and Pardi, A. (1996) A network of heterogeneous hydrogen bonds in GNRA tetraloops, *J. Mol. Biol. 264*, 968−980.
43. Ladame, S., Castilho, M. S., Silva, C. H., Denier, C., Hannaert, V., Perie, J., Oliva, G., and Willson, M. (2003) Crystal structure of *Trypanosoma cruzi* glyceraldehyde-3-phosphate dehydrogenase complexed with an analogue of 1,3-bisphospho-D-glyceric acid, *Eur. J. Biochem. 270*, 4574−4586.
44. Gadd, R. E., and Henderson, J. F. (1970) Studies of the binding of phosphoribosyl pyrophosphate to adenine phosphoribosyltransferase, *J. Biol. Chem. 245*, 2979−2984.
45. Hirao, I., Yoshizawa, S., and Miura, K. (1993) Stabilization of mRNA in an *Escherichia coli* cell-free translation system, *FEBS Lett. 321*, 169−172.
46. Hirao, I., Ishida, M., Watanabe, K., and Miura, K. (1990) Unique hairpin structures occurring at the replication origin of phage G4 DNA, *Biochim. Biophys. Acta 1087*, 199−204.

BI0474362